Desalination and Water Treatment
www.deswater.com

doi: 10.5004/dwt.2020.25726

191 (2020) 400–416
July

Removal of basic fuchsin from aqueous solutions by low-cost peanut shells adsorbent in a fixed bed column

Amina Lahmar[a], Zhour Hattab[a,*], Radia Zerdoum[b], Amina Berredjem[b], Ridha Djellabi[a], Kamel Guerfi[a]

[a]*Laboratory of Water Treatment and Valorization of Industrial Wastes, Department of Chemistry, Faculty of Sciences, Badji-Mokhtar University, B.P.12, Annaba 23000, Algeria, emails: zoumourouda20012000@yahoo.fr (Z. Hattab), anima.lahmar@gmail.com (A. Lahmar), ridha.djellabi@yahoo.com (R. Djellabi), k_guerfi@yahoo.fr (K. Guerfi)*
[b]*Science and Technology Laboratory of Water and Environment, Faculty of Science and Technology, Mohammed Cherif Messadia University, Souk Ahras 41000, Algeria, emails: environnement2004@yahoo.fr (R. Zerdoum), y_berredjem@yahoo.fr (Y. Berredjem)*

Received 8 August 2019; Accepted 21 February 2020

ABSTRACT

The current study aims to valorize a raw peanut shell powder (PSP) as an innovative biomaterial for the recovery of basic fuchsin (BF) from the water via a dynamic adsorption process. In particular, the influence of some operating parameters such as flow rate, bed height, BF concentration, pH of the solution, ionic strength and temperature on the breakthrough curve was studied. The Fourier transform infrared spectroscopy analysis confirms the dominant presence of cellulose, hemicellulose, lignin and xylene in PSP which is in good agreement with the X-ray diffraction analysis. Scanning electron microscopy images show that PSP has a morphology rich with hollow cavities with a high roughness that is favorable to the binding of organic molecules. The value of the Zeta potential (2.30 mV) confirms a positive charge of the material surface which is in good agreement with the curve pH_{PZC} (PZC – point of zero charge). The adsorption tests showed that overall, an optimal adsorption efficiency of 98% can be achieved for a flow rate of 4 mL min^{-1}, an initial concentration of 5 mg L^{-1}, a bed height of 55 mm, a pH 6 and a temperature of 298 K. Four kinetic models (Thomas, Yoon–Nelson, Bohart–Adams, and Wolborska) were proposed to predict the breakthrough curves using non-linear regression and determine the characteristic parameters of the column, namely the kinetic constants of Thomas (3.14×10^{-3} ml mg^{-1} min^{-1}) and Yoon–Nelson (13.62×10^{-3} min^{-1}), the sorption rate coefficient of Bohart–Adams (2.86×10^{-3} ml mg^{-1} min^{-1}) and the external mass transfer kinetic coefficient of Wolborska (15.90 min^{-1}). The results indicate that the four proposed models are adequate for describing the breakthrough curve and that the data is in good agreement with the bed depth service time model with some limitations.

Keywords: Peanut shells; Basic fuchsin; Dynamic adsorption; Non-linear regression; Modeling

1. Introduction

Access to purified and safe drinking waters has become a worldwide issue. To address this challenge, industrial demand has increased for innovative and improved water treatment methods [1]. The intensive use of dyes in varying industries often results in high polluted wastewater; and therefore, such colored wastewater can cause serious environmental and health issues [2,3].

Basic fuchsin (BF), triaminotriphenylmethane ($C_{20}H_{20}ClN_3$) and its chemical structure is shown in Fig. 1 [4] is widely used as a coloring agent for textile materials, muscles, collagen, leather, mitochondria, and tuberculosis bacilli [5]

* Corresponding author.

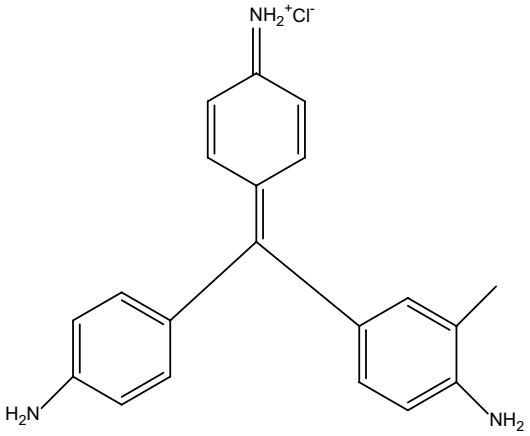

Fig. 1. Chemical structure of basic fuchsin.

which makes it one of the most common dye in industrial effluents [5]. It is important to highlight that the contact with dyes usually causes a wide range of toxicity [6] such as gastrointestinal irritation with nausea, vomiting, and diarrhea, irritation to the respiratory tract [7], severe eye and skin irritation [8] affect the nervous system with headache, dizziness, lethargy, and muscle contraction. Its toxicity includes carcinogenic and has also mutagenic effects [9], damage to the organs such as blood, liver, spleen, and thyroid [10]. It has fungicidal, anesthetic and bactericidal properties [11,12]. Various processes for removing dye from wastewater have been used [13–21], including physicochemical and biological processes that are difficult to manage and costly or less efficient. For this reason, the search for economical adsorbents, preferably derived from locally available waste, has, therefore, become one of the main axes of research [22]. Biosorption technology offers an efficient and economical alternative compared to the conventional decontamination methods [23–28]. It offers numerous advantages such as low cost, high efficiency, no additional nutrients required, minimization of chemical or biological sludge and the possibility of effluent recovery [29–36]. With regard to the elimination of BF, and to the best of authors' knowledge, little research has recently been reported in the literature using different techniques and adsorbents such as dead biomass of *Aspergillus niger* [37], biosorbent Citrobacter [38], treated malted sorghum mash [39], silver colloid [40], *Zizania latifolia* [41], Euryale Ferox Salisbury seed shell [42], biogenic apatite (fish bones) [43], activated leather waste [44], mesoporous carbons [45], modified cellulose [46], modified iron oxide nanoparticles [47]. The accumulation of agro-industrial waste has caused two major problems: the occupation of land space and pollution due to the dumping of this waste. In this context, the use of agro-industrial waste as adsorbents for the removal of dyes represents a beneficial combination of economic and environmental considerations.

Peanut shells are a by-product of peanut processing and have the advantages of a wide range of sources, high production volumes, low costs and are environmentally friendly. Their use as a bioadsorbent has attracted increasing interest in recent years due to their high adsorption capacity. Only a small proportion of the peanut shells are recycled as fuel or food, while most of peanut shells are discarded or burned, resulting in a waste of resources. Several studies deal with the use of peanut shells as adsorbent materials or activated carbon made from peanut shells have been reported for the removal of dyes, heavy metals and other pollutants [48].

The objective of this work was the removal of BF from aqueous solutions by peanut shell powder (PSP) in fixed-bed columns. The influence of some influencing factors such as flow rate, bed height, concentration, temperature, pH and ionic strength were investigated during the column tests.

2. Materials and methods

Peanut shell was recovered from local agricultural fields in southern Algeria's Wadi Souf region. Hydrogen chloride (HCl), sodium hydroxide (NaOH), sodium chloride (NaCl) and BF were purchased from Sigma-Aldrich-Fluka (Saint-Quentin, Fallavier, France).

2.1. Preparation of adsorbent

Peanut shells were washed with distilled water to remove impurities, dried in open air than in an oven at 105°C for 24 h to remove residual moisture. The as-obtained sample was ground in an electric grinder and then sieved using a sieve (Afnor, London, UK). Only particles with diameters between 315 and 500 μm were used for further studies.

2.2. Characterization of peanut shell

Morphological observations were performed by scanning electron microscopy (SEM) using (Quanta 200 Field Electron and Ion Company) combined with energy-dispersive X-ray spectroscopy (EDX). The EDX analysis was used for elemental composition present in the sample. Functional groups were identified by Fourier transform infrared spectroscopy (FTIR) using IR^{-1} affinity in combination with a single attenuated total reflectance reflection. The structure and purity were checked by X-ray diffraction (XRD) using Rigaku Ultima IV, (Neu-Isenburg, Germany) diffractometer equipped with copper Kα (λ = 1.5460 Å) radiation source, operating at 40 kV and 40 mA, with a scanning rate of 0.01 min^{-1} and 2θ range 0°–70°. Specific surface area Brunauer–Emmett–Teller (BET) which determines the porosity of adsorbent, was determined from nitrogen adsorption isotherm at 77 K using NOVA Quantachrome, (Boynton Beach, US) (NOVA 1000e). Before measurement, each sample was degassed at 150°C for 1 h in a nitrogen atmosphere. Zeta potential measurement which reflects the electrical potential at the interface between the adsorbent particles and the adjacent liquid was realized using a Zetasizer 2000, Malvern Co., (England) instrument equipped at a temperature of 21°C and a pH of 5.63, in order to measure the strength of attractive/repulsive interactions between particles and to obtain information on surface properties of suspended particles. To check the thermal stability of PSP, thermogravimetric analysis (TGA) and differential scanning calorimetry (DSC) were carried out on METTLER TOLEDO, (Columbus, Ohio, US), STARe TGA/DSC 3 +

System, at a heating rate from 10°C min^{-1} (30 mL min^{-1}) up to 600°C under N_2 flow gas atmosphere. Point of zero charge (PZC) to determine the value at which acid or basic functional groups no longer contribute to the pH of the solution, was performed according to the method described by Ponnusami et al. [49]. The PZC value of PSP was obtained from the curve representing pH_f–pH_i values as a function of pH of PSP. PZC value corresponds to the intersection value with the abscissa axis, where ΔpH = 0.

2.3. Column adsorption experiments

Column experiments were performed in a glass column (diameter: 11 mm, length: 300 mm).

The residual BF concentration was determined at a wavelength of λ_{max} = 546 nm using a UV-Vis spectrophotometer (JENWAY 7315, Staffordshire, England).

2.4. Analysis of experimental data

The adsorption failure profiles of BF are obtained from $\frac{C_t}{C_0} = f(t)$, where C_t and C_0 represent the effluent and influence concentrations, respectively, t is the service time. The volume of treated effluent is represented by the following equation [50].

$$V_{eff} = F(t_e) \tag{1}$$

where F (mL min^{-1}) and t_e (min) is the entry flow rate and saturation time.

The total amount of BF adsorbed in the PSP bed column is calculated using the following equation [51]:

$$q_{total} = \frac{F}{1{,}000} A = \frac{F}{1{,}000} \int_t^{t=total} C_{ads}\, dt \tag{2}$$

C_{ads} = (C_0 – C_t), the breakthrough is obtained by tracing $C_{ads} = f(t)$ where A is the area under the curve $C_{ads} = f(t)$, C_0 is the initial concentration of BF and C_t is the BF concentration of the effluent, respectively.

Meanwhile, q_{exp} (mg g^{-1}) is calculated by dividing the total quantity by the mass of biosorbent m [52]:

$$q_{exp} = \frac{q_{total}}{m} \tag{3}$$

In addition, N_{exp} (mg L^{-1}) can be calculated from the adsorption capacity as follows [53]:

$$N_{exp} = q_{exp} \frac{m}{V} \tag{4}$$

where V (mL) is the volume of the adsorbent.

The quantities of adsorbate passing through the column W_{total} (mg) are determined as follows [54]:

$$W_{total} = \frac{C_0 q t_{total}}{1{,}000} \tag{5}$$

The adsorbate absorption percentage is calculated by:

$$R\% = \frac{q_{total}}{W_{total}} \times 100 \tag{6}$$

2.5. Kinetic adsorption models

In this study, five theoretical models, Thomas, Yoon–Nelson, Bohart–Adams, Wolborska, and bed depth service time (BDST), were applied to predict the failure curves.

2.5.1. Thomas model

This model is usually applied to the progress of biosorption where external and internal diffusion limitations are absent [55]. It is used to calculate the adsorption rate constant and the concentration in the solid phase of the dye on the adsorbent from the continuous mode studies. The model is represented by the following form:

$$\frac{C_t}{C_0} = \frac{1}{1 + \exp\left(\frac{K_{th} m q_{th}}{U} - C_0 K_{th} t\right)} \tag{7}$$

The kinetic coefficient K_{th} and the absorption capacity q_{th} can be determined from a graph of $\frac{C_t}{C_0} = f(t)$ for a given flow rate using a non-linear regression analysis.

2.5.2. Yoon–Nelson model

Yoon–Nelson developed a simple model of adsorption and penetration of adsorbate vapor/gas onto activated carbon [56]. It is based on the assumption that the rate of decrease in the probability of the adsorbate molecule is proportional to the probability of the adsorbate penetrating the adsorbent. This model is less complicated than the other models because it does not require detailed data on the type of adsorbent, the characteristics of the adsorbent and the physical properties of the adsorption bed. For a one-component system, it is expressed as follows [56]:

$$\frac{C_t}{C_0} = \frac{1}{1 + e^{K_{YN}(\tau - t)}} \tag{8}$$

where K_{YN} is the constant of speed (min^{-1}), τ is the time required for the passage of 50% sorbate (min) and t is the time (min).

2.5.3. Bohart–Adams model

This model is used to describe the initial part of the breakthrough curve, and be defined by the following equation [57]:

$$\frac{C_t}{C_0} = \exp\left(K_{BA} C_0 t - K_{BA} N_0 \frac{Z}{U}\right) \tag{9}$$

where C_0 and C_t (mg L^{-1}) are the initial and critical concentrations, K_{BA} (L mg^{-1} min^{-1}) is the sorption rate coefficient,

N_0 (mg L^{-1}) is the sorption capacity per unit volume, Z (mm) is the bed depth, U (mm min^{-1}) is the linear velocity and t (min) is the time.

2.5.4. Wolborska model

Wolborska proposed a model based on the general mass transfer equations for the diffusion mechanism in the range of the low-concentration breakthrough curve. It can be used to experimental data describing the initial part of the breakthrough curve and can be defined as follows [58]:

$$\frac{C_t}{C_0} = \exp\left(\frac{\beta_a C_0}{N_0} t - \frac{\beta_a Z}{U}\right) \tag{10}$$

where β_a (min^{-1}) is the external mass transfer kinetic coefficient, and N_0 (mg L^{-1}), is the saturation concentration of the fixed bed reactor.

2.5.5. BDST model

This model was proposed by Bohart–Adams in 1920 [57]. It is based on the assumption that the adsorption rate is controlled by the surface reaction between the adsorbate and the unused capacity of the adsorbent [59]. It is used to estimate the bed depth required for a given operating time. A linear relationship between bed depth and operating time is given by the following equation [59]:

$$t_b = \frac{N_0'}{C_0 U} Z - \frac{1}{K_{BA} C_0} \ln\left(\frac{C_0}{C_b} - 1\right) \tag{11}$$

where t_b (min) is the operating time and N_0' (mg L^{-1}) the sorption capacity, C_0 (mg L^{-1}) is the initial concentration, U (mm min^{-1}) is the surface velocity of the fluid and Z (mm) the height of the fixed bed, C_b (mg L^{-1}) the specific breakthrough concentration.

2.6. Test of kinetic models

The parameters of different kinetic models were obtained using non-linear analysis. The error functions were used to determine the error distribution between the predicted and experimental values. The conformity of the model is better when the error is lower [60]. The coefficient of determination, which represents the percentage variability of the dependent variable (the variance around the mean), is used to analyze the degree of fit of isothermal and kinetic models to experimental data [61]. The mathematical formulas for the Chisquare analysis χ^2 and estimated standard deviation (ESD) are given below [62]:

$$\chi^2 = \sum_{i=1}^{n} \frac{\left[\left(\frac{C_t}{C_0}\right)_c - \left(\frac{C_t}{C_0}\right)_e\right]^2}{\left(\frac{C_t}{C_0}\right)_c} \tag{12}$$

$$\mathrm{ESD} = 100 \times \left\{ \sum \frac{\left[\left(\left(\frac{C_t}{C_0}\right)_c - \left(\frac{C_t}{C_0}\right)_e\right) \Big/ \left(\frac{C_t}{C_0}\right)_e\right]^2}{N-1} \right\}^{1/2} \tag{13}$$

where $\left(\frac{C_t}{C_0}\right)_c$ is the ratio of effluent and influent BF concentrations according to dynamic models, and $\left(\frac{C_t}{C_0}\right)_e$ is the ratio of effluent and influent BF concentrations according to experience, respectively, and N is the number of experimental data.

3. Results and discussion

3.1. Structural analysis

3.1.1. FTIR analysis

The peaks observed in FTIR spectra for PSP before and after adsorption are assigned to various groups and bands according to their wavenumbers (cm^{-1}), Fig. 2. The bands at 3,344 and 2,922 cm^{-1} are attributed to –OH and C–H, respectively (groups present in the lignin) while the band at 2,160 cm^{-1} are ascribed to C–C. The bond C=O of hemicellulose and C=C are observed at 1,745 and 1,649 cm^{-1} whereas C=O of the aromatic ring of lignin appears at 1,586 cm^{-1}. The bands detected at 1,260 cm^{-1} corresponds to the CO of lignin and xylene. The band at 1,024 cm^{-1} is assigned to C–OH of hemicellulose and cellulose [63], while that at 656 cm^{-1} is due to the vibration of the aromatic compounds of lignin. On the other hand, after the adsorption of BF, there is a decrease in the intensity of the following bonds C–H, and C=O corresponding to the bands 2,922 and 1,745 cm^{-1}, respectively. This decrease could be due to the chemical interactions between the BF dye molecules and the surface of the PSPs [64]. On the other hand, a peak at 1,360 cm^{-1} corresponds to the stretching of C–N appeared in the PSPs spectrum after BF adsorption [44]. Additionally, it can be observed a doublet due to the primary amine $–NH_2$ and the secondary amine =NH appeared at 3,344 and 3,229 cm^{-1} [65–67] which are partially masked by the OH band [42], suggesting the fixation of BF onto PSP surface.

3.1.2. EDX analysis

According to Fig. 3, the highest amounts corresponded to the carbon and the oxygen prove the organic nature of the adsorbent [68,69].

3.1.3. XRD analysis

The XRD pattern shown in Fig. 4 reveals a typical spectrum of cellulosic material. Two peaks are observed; the main peak at 2θ = 22° associated with the presence of highly organized crystalline cellulose, and a secondary peak at 2θ = 16° which is often associated with a less organized polysaccharide structure. This result is confirmed by the

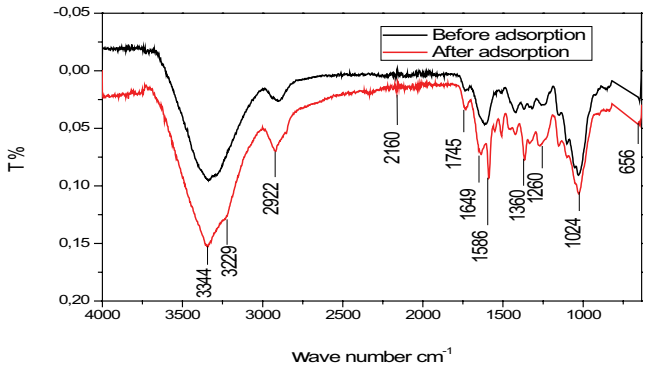

Fig. 2. FTIR spectra of PSP before and after adsorption of BF.

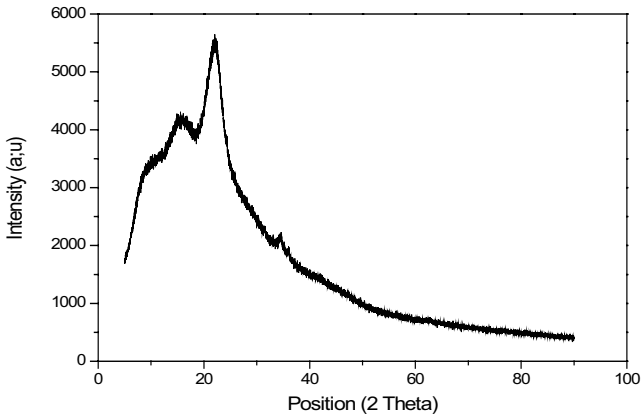

Fig. 4. XRD analysis results for the PSP before adsorption.

FTIR analysis where cellulosic peaks have been identified, it can, therefore, be concluded that PSP used is semi-amorphous, which is in good agreement with the literature [70,71].

3.2. Microstructural analysis

3.2.1. SEM observations

The textural morphology was observed by SEM analysis and the obtained images with different magnifications are shown in Fig. 5. PSP exhibits mesoporous architectures with hollow cavities which can boost the fixation of the high amount of dyes molecules [64].

3.3. Thermal analysis

3.3.1. TGA analysis

The TGA of the PSP is shown in Fig. 6. Five weight loss phases are distinct in the curve. The first phase in the temperature range (25°C–110°C) corresponds to a loss of about 8.98% of the sample weight due to physically absorbed non-dissociative water molecules as well as water maintained at the surface by hydrogen bonding (dehydration) [72]. The second weight loss is 9.02% in the temperature range of (110°C–250°C) which corresponds to the depolymerization of hemicellulose and the breakdown of glycosidic bonds [73]. The third phase is between (250°C–350°C) with the highest loss of 41.03%, it indicates the degradation of celluloses (a larger crystal structure requires a higher degradation temperature). The cleavage of the glycosidic bonds of cellulose, leading to the formation of H_2O, CO_2, alkanes and other hydrocarbon derivatives. The fourth phase corresponds to the degradation of 15.38% of the lignin at (350°C–440°C). In the temperature range (440°C–600°C), there is a fifth weight loss of 25.59%, corresponding to carbonaceous residues [74–76].

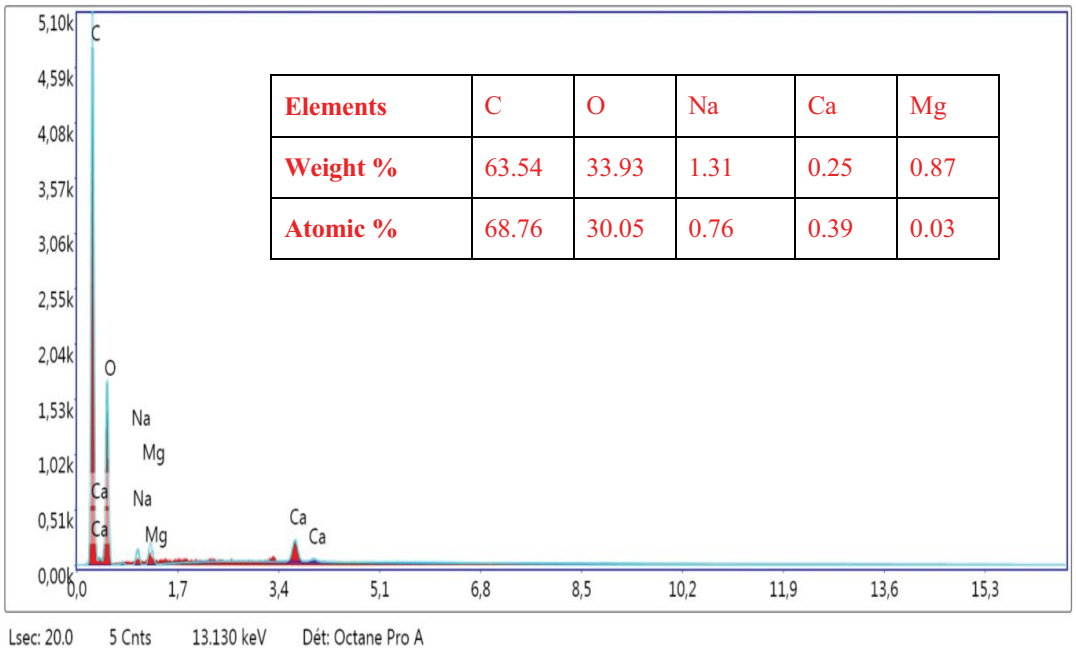

Elements	C	O	Na	Ca	Mg
Weight %	63.54	33.93	1.31	0.25	0.87
Atomic %	68.76	30.05	0.76	0.39	0.03

Fig. 3. EDX profile of PSP.

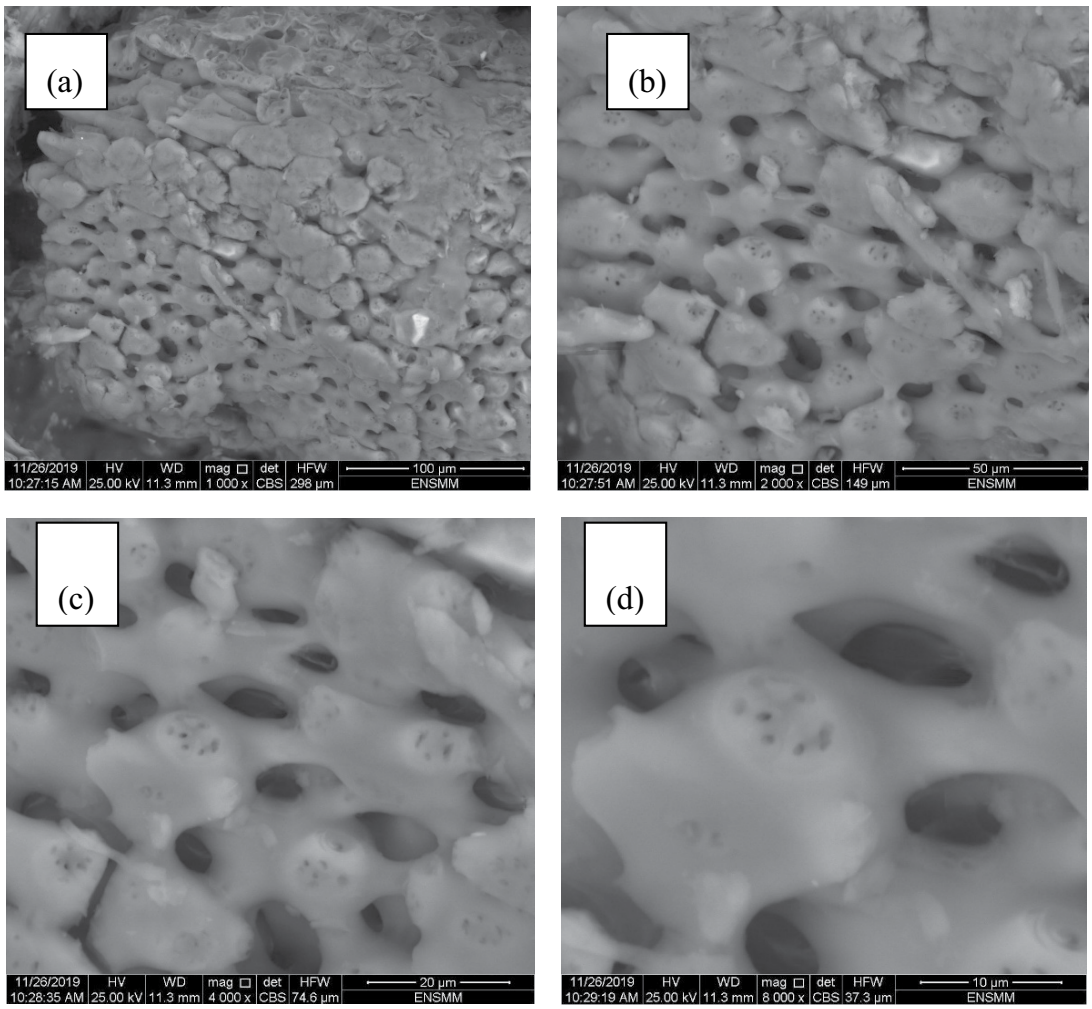

Fig. 5. SEM images of PSP before BF adsorption: (a) ×1,000; (b) ×2,000; (c) ×4,000; and (d) ×8,000.

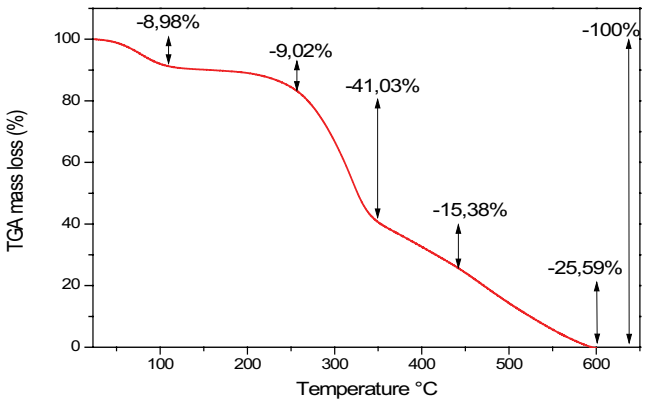

Fig. 6. TGA analysis of PSP.

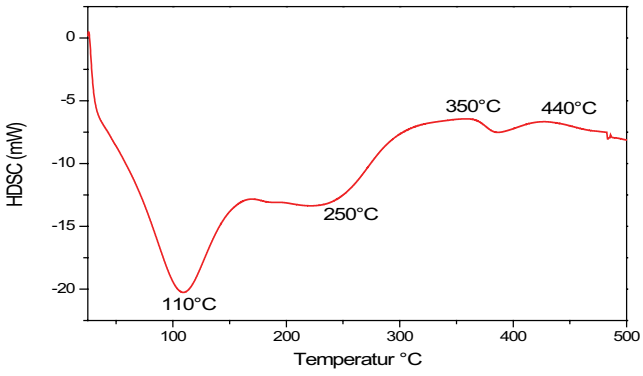

Fig. 7. DSC analysis of PSP.

3.3.2. DSC analysis

The results of DSC analysis from 10°C to 500°C are shown in Fig. 7. Different endothermic peaks were produced confirming the different losses of weights observed in TGA analysis [77].

3.4. BET and zeta potential measurements

The results of the specific surface area BET, the porosity measurements and the zeta potential of the PSP are presented in Table 1. The zeta potential measurement, which reflects the electrical potential at the interface between the PSP particles and the adjacent liquid, shows that PSP has a

positive zeta potential. This indicates that the PSP surface is positively charged in the water at pH 5.63, the acid pH causes the protonation of hydroxyl and carboxyl groups and would make the surface positive to a certain extent for a biomaterial containing cellulose and hemicellulose [78].

PSP exhibits a surface area of 4.92 $m^2 g^{-1}$ and a pore diameter of 41.22 (nm) as shown by SEM images also (mesoporous type according to UIPAC) [79].

The porous nature of PSP was determined using the N_2 adsorption–desorption isotherms, as shown in Fig. 8.

Table 1
Specific surface area and pore distribution of PSP

Parameters	PSP
BET surface area ($m^2 g^{-1}$)	4.92
Total pore volume ($cm^3 g^{-1}$)	0.007807
Average pore diameter (nm)	41.22
Zeta potential (mV)	2.30
Particle density (g cm^{-3})	2.28

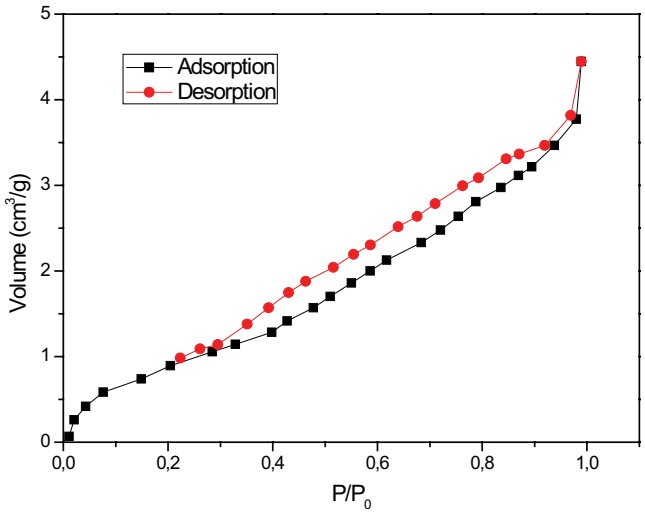

Fig. 8. N_2 adsorption–desorption isotherms of PSP.

These can be classified as type IV isotherms, which are characteristic of mesoporous material [48,80].

3.5. Point of zero charge

The pH_{PZC} of an adsorbent is a very important characteristic that determines the value at which acid or basic functional groups no longer contribute to the pH of the solution [81]. Fig. 9 shows that pH_{PZC} of PSP is 6.77, which implies that its surface is positively charged at pH < 6.77 and negatively charged at pH > 6.77. This is in agreement with the results of the zeta potential.

3.6. Adsorption of BF by PSP

3.6.1. Effect of low rate

According to Fig. 10 and Table 2, the increase in flow rate causes the decrease in operating times t_b and t_e [82] and leads to the increase in volume, which in turn, increases adsorbed capacity [83], this phenomenon can be explained by the porous nature of PSP (PSP is mesoporous-type revealed in BET with structural hollow cavities in which the pollutant can be fixed), The increase in flow rate favors the mass transfer rate between the solute and the biosorbent, however, we can conclude that the contact time is sufficient for the mass transfer between the adsorbate and biomass [84].

3.6.2. Effect of bed height

The results are shown in Fig. 11 and summarized in Table 2 demonstrate that the equilibrium sorption capacity decreases with increasing bed height. This phenomenon is probably explained by the diffusion of the molecules of BF dye into the pores of the adsorbent which can be transported to the surface. These results are in good agreement with some studies in the literature [83,85,86].

3.6.3. Effect of initial concentration

The results presented in Fig. 12 indicates that with increasing the initial BF concentration the adsorption capacity increases, thereby resulting in a decrease in penetration

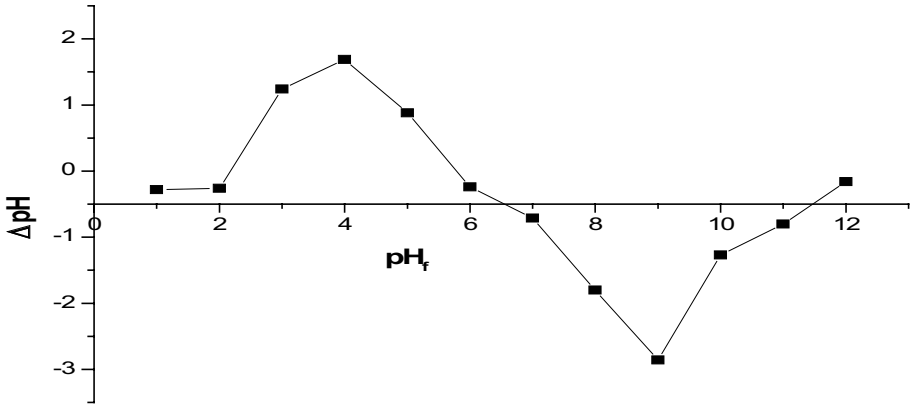

Fig. 9. Point of zero charge of PSP.

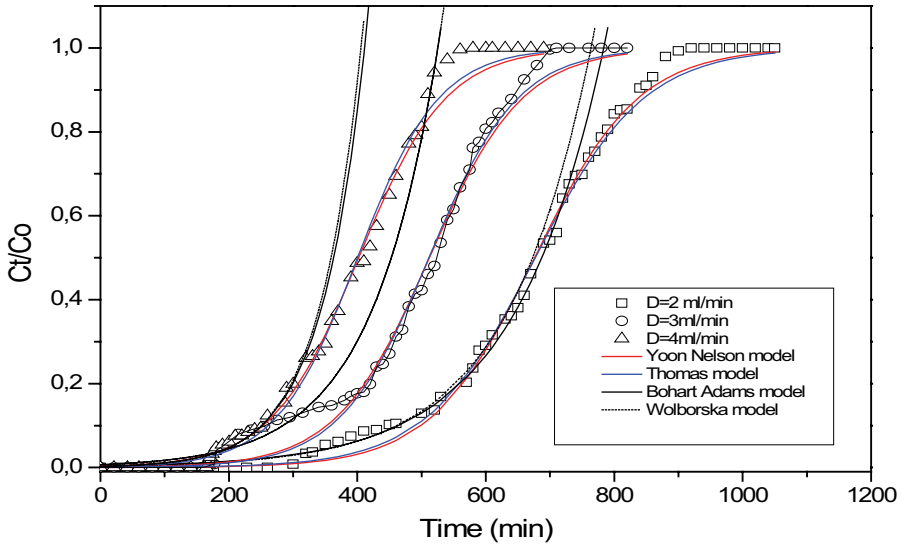

Fig. 10. Comparison of experimental and predicted penetration curves obtained at different flows according to the models studied for BF adsorption by PSP. (pH = 6 ± 0.1, C_0 = 10 mg L^{-1}, Z = 25 mm, and T = 298 K).

Table 2
Conditions and the results for the fixed-column experiments

C_0 (mg L^{-1})	Z (mm)	F (mL min^{-1})	pH	T (K)	NaCl (N)	t_b (min)	t_{total} (min)	V_{eff} (mL)	W_{total} (mg)	q_{total} (mg)	q_{exp} (mg g^{-1})	R (%)
10	15	4	6	298	0	84	460	1,840	21.2	12.18	40.60	57.45
10	25	4	6	298	0	250	515	2,060	23.2	15.97	31.94	68.85
10	35	4	6	298	0	350	650	2,600	28.8	20.62	29.46	71.62
5	25	4	6	298	0	365	645	2,580	14.2	10.64	21.29	74.97
15	25	4	6	298	0	225	430	1,720	28.5	21.18	42.37	74.33
10	25	2	6	298	0	450	840	1,680	20.0	13.39	26.80	66.99
10	25	3	6	298	0	260	655	1,965	21.3	14.92	29.85	70.08
10	25	4	8	298	0	265	610	2,440	26.8	18.65	37.30	69.59
10	25	4	4	298	0	99	380	1,520	16.0	9.78	19.56	61.14
10	25	4	6	318	0	295	770	3,080	35.6	22.52	45.13	63.39
10	25	4	6	308	0	260	600	2,400	28.8	17.67	35.34	61.35
10	25	4	6	298	0.1	22	160	640	9.0	3.44	6.88	38.23
10	25	4	6	298	0.01	140	497	1,988	22.4	13.75	27.50	61.38

and saturation times. This is due to the rapid recovery of all adsorption sites [75] and a greater mass transfer in the adsorption process, which leads to the treatment of a small volume of BF solution [87].

3.6.4. Effect of initial solution pH

Fig. 13 illustrates the evolution of adsorption capacity as a function of solution pH. It can be observed that in the pH range of (4–8), a significant increase in the adsorption capacity in the basic medium is achieved. This result could be explained [88] by the cellulosic behavior of the adsorbent which, in aqueous medium and given the formation of the groups RO^- according to the acid-base reaction of the hydroxide groups of the cellulose, is negatively charged [89]:

$$ROH + H_3O^+ \rightarrow ROH_2^+ + H_2O \quad (14)$$

$$ROH + H_2O \rightarrow RO^- + H_3O^+ \quad (15)$$

$$ROH + OH^- \rightarrow RO^- + H_2O \quad (16)$$

Therefore it is clear that an increase in pH promotes the formation of the group RO^- hence the development of a negative electrical charge on the surface of the peanut shells. This charge presents with respect to the BF (R^+, Cl^-) an electrostatic attraction due to the positive charge which it carries in solution (R^+, $Cl^- \rightarrow R^+ + Cl^-$).

$$RO^- + R^+ \rightarrow RO^-R^+ + H_2O \quad (17)$$

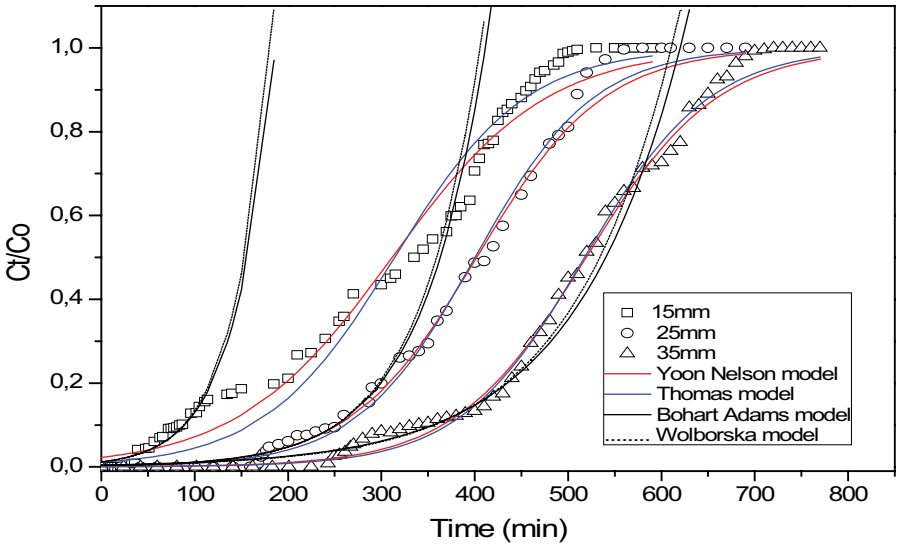

Fig. 11. Comparison of experimental and predicted penetration curves obtained at different bed heights according to the models studied for the adsorption of BF by PSP. (pH = 6 ± 0.1, C_0 = 10 mg L^{-1}, F = 4 mL min^{-1} and T = 298 K).

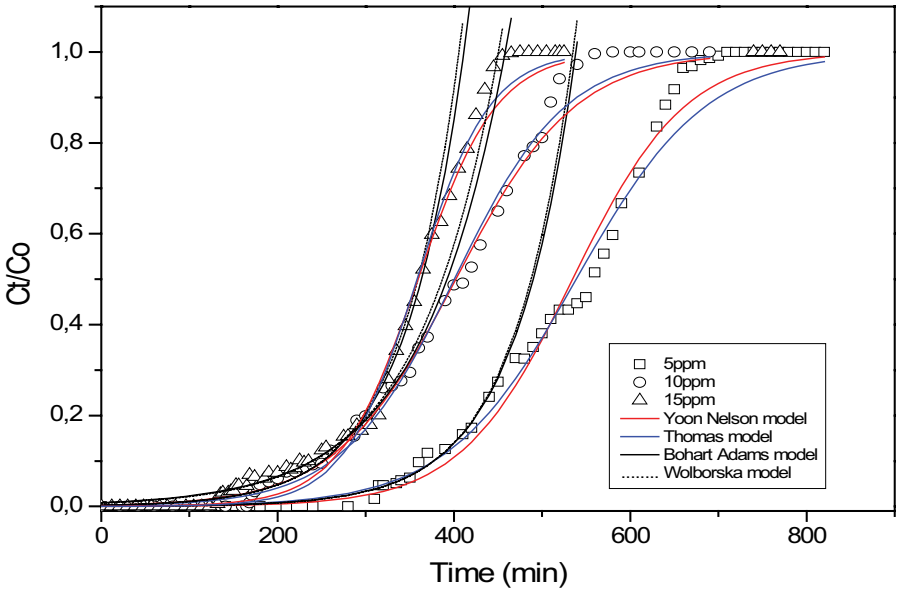

Fig. 12. Comparison of experimental and predictive breakthrough curves obtained at different BF concentrations, according to the models studied for the adsorption of BF by PSP. (pH = 6 ± 0.1, Z = 25 mm, F = 4 mL min^{-1}, and T = 298 K).

Several authors have observed similar effects of pH on the adsorption of dyes on various adsorbents [90–92].

3.6.5. Effect of ionic force

Ionic strength has a significant role in the structure of the electric double layer (EDL) of a hydrated particle. The thickness of the EDL decreases as the ionic strength increases, causing a decrease in adsorption [93].

The increase in ionic strength results in a decrease in breakthrough and saturation time. The NaCl salt releases Na^+ cations in solutions, these ions competing with BF cations to bind to the active PSP sites, which is reflected in the decrease in adsorption capacity as shown in Fig. 14 and Table 2. These results are in agreement with the results reported in different adsorption studies using different types of bioadsorbents such as lignocellulosic, membrane and silica [61,93,94].

3.6.6. Effect of temperature

According to Fig. 15, the adsorption capacity of BF increases at higher temperatures. The increase in temperature would increase the mobility of the dye ions and produce a swelling effect in the internal structure of the natural adsorbate, allowing the dye molecules to penetrate

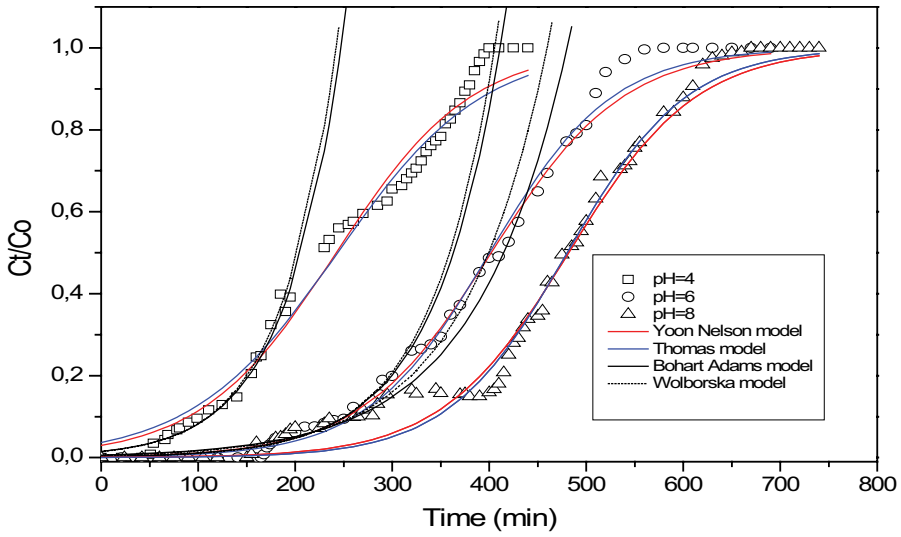

Fig. 13. Comparison of experimental and predictive breakthrough curves obtained at different pH of BF, according to the models studied for the adsorption of BF by PSP. (C_0 = 10 mg L^{-1}, F = 4 mL min^{-1}, Z = 25 mm, and T = 298 K).

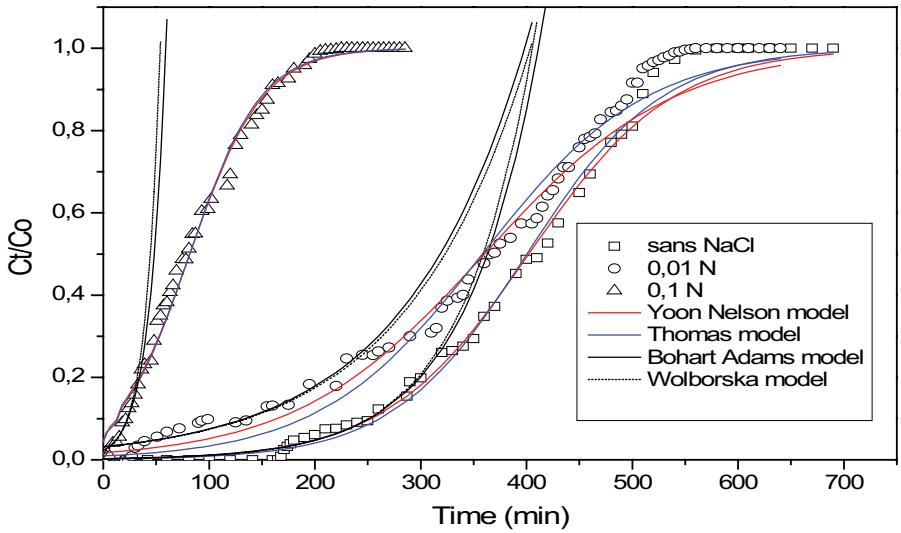

Fig. 14. Comparison of experimental and predictive breakthrough curves obtained at different NaCl concentrations, according to the models studied for BF adsorption by PSP. (C_0 = 10 mg L^{-1}, Z = 25 mm, F = 4 mL min^{-1}, pH = 6 ± 0.1, and T = 298 K).

Table 3
Conditions and the results for the fixed-column experiment of optimization of effects

C_0 (mg L^{-1})	Z (mm)	F (mL min^{-1})	pH	T (K)	NaCl (N)	t_b (min)	t_{total} (min)	V_{eff} (mL)	W_{total} (mg)	q_{total} (mg)	q_{exp} (mg g^{-1})	R (%)
5	25	4	6	298	0	365	645	2,580	14.2	10.64	21.29	74.97
5	45	4	6	298	0	415	700	2,800	5.0	14.48	16.09	96.54
5	55	4	6	298	0	490	740	2,960	16.8	16.48	14.98	98.13

further. Therefore, the adsorption capacity should be largely dependent on the chemical interaction between the functional groups on the surface of the adsorbent and adsorbate and should increase with the rise of temperature. This can be explained by an increase in the rate of diffusion of the adsorbate into the pores [95]. Thus, the increase in adsorption capacity can be translated into the creation of new active sites. This indicates that the adsorption in this system is an endothermic process [96]. Similar results were observed by Ozer et al. and Song et al. [97,98].

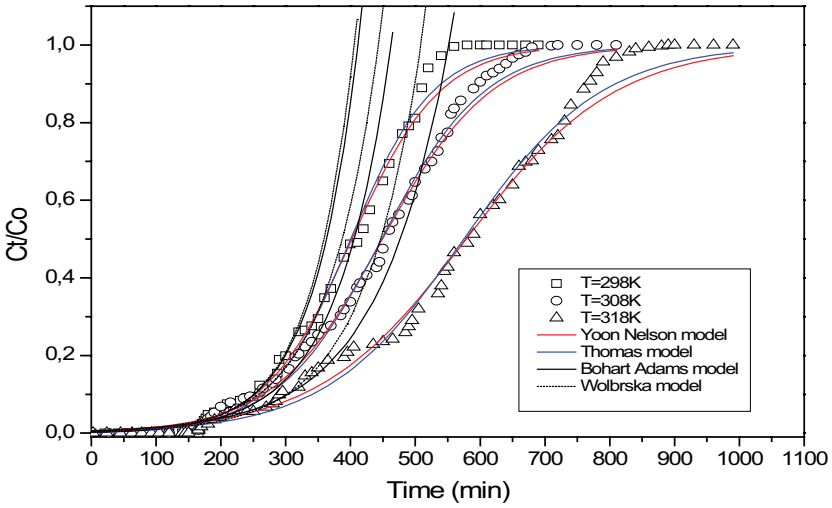

Fig. 15. Comparison of experimental and predictive breakthrough curves obtained at different BF temperatures, according to the models studied for the adsorption of BF by PSP. (C_0 = 10 mg L^{-1}, F = 4 mL min^{-1}, Z = 25 mm, and pH = 6 ± 0.1).

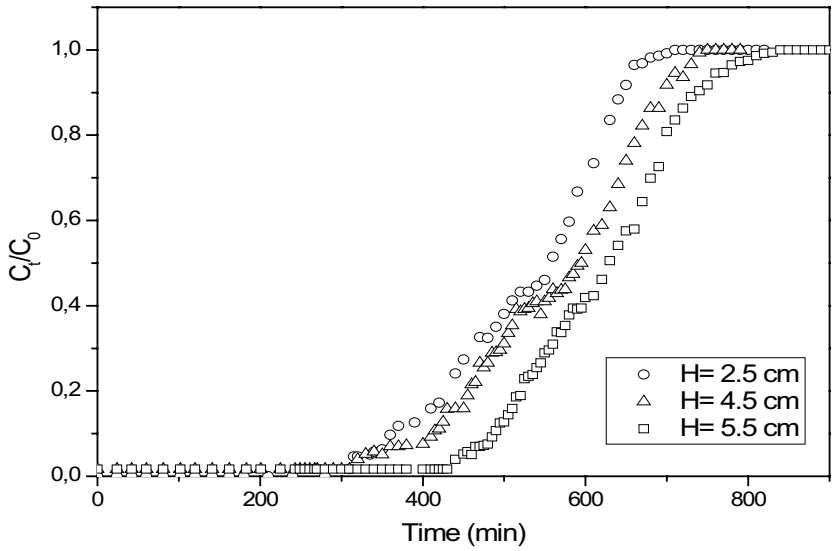

Fig. 16. Optimization of effects. (C_0 = 5 mg L^{-1}, F = 4 mL min^{-1}, pH = 6 ± 0.1, and T = 298 K).

3.7. Optimization of effects

The adsorption capacity of the PSP adsorbent has been optimized by optimizing the different effects studied for the removal of basic fuchsin (Fig. 16 Table 3). The adsorption tests showed that overall, an optimal adsorption efficiency of 98% can be achieved for a flow rate of 4 mL min^{-1}, an initial concentration of 5 mg L^{-1}, a bed height of 55 mm, a pH 6 and a temperature of 298 K.

4. Modeling

4.1. Thomas and Yoon–Nelson models

According to Table 4, it can be seen that the adsorption capacities calculated from Thomas' model and τ values from Yoon–Nelson are very close to the value obtained experimentally. It is also interesting to observe that the values of R^2 coefficients for both models are greater than 0.97 as well as the error value for the total effects does not exceed 5%. $\frac{K_{YN}}{C_0}$ is equal to K_{th}, which proves that the expression of Thomas's solution is equivalent to the Yoon–Nelson relationship. In addition, it should be noticed that the Thomas speed constant increases with increasing the flow rate while it decreases with increasing dye concentration. This may be due to the driving force of adsorption and the difference in concentration between the dye in the solution and the dye on the adsorbent [99]. For Yoon–Nelson's model, the speed constant increases and τ decreases with increasing the flow rate. This may be because a higher flow rate would allow the adsorption equilibrium to be reached at early stage of the adsorption process. It can be argued that Thomas and Yoon–Nelson's models are appropriate to describe the adsorption of BF in the fixed bed PSP. Similar results were reported in the literature by Singh and al [100].

Table 4
Parameters of Thomas and Yoon–Nelson models for BF adsorption by PSP at different conditions using non-linear regression

						Thomas model					Yoon–Nelson model				
C_0 (mg L^{-1})	Z (mm)	F (mL min^{-1})	pH	T (K)	NaCl (N)	$K_{th} \times 10^3$ (ml mg^{-1} min^{-1})	q_{th} (mg g^{-1})	q_{exp} (mg g^{-1})	R^2	$\chi^2 \times 10^3$	ESD (%)	$K_{YN} \times 10^3$ (min^{-1})	τ (min)	τ_{exp} (min)	R^2	$\chi^2 \times 10^3$	ESD (%)
10	15	4	6	298	0	1.21 ± 0.04	41.54 ± 0.49	40.60	0.9826	2.64	5.13	14.27 ± 0.33	314.18 ± 3.49	335	0.9776	1.99	4.46
10	25	4	6	298	0	1.58 ± 0.04	32.03 ± 0.16	31.94	0.9942	0.86	2.94	14.75 ± 0.39	402.12 ± 1.86	410	0.9923	0.65	2.56
10	35	4	6	298	0	1.50 ± 0.02	29.58 ± 0.07	29.46	0.9949	0.73	2.71	14.27 ± 0.33	519.35 ± 1.70	515	0.9925	0.66	2.57
5	25	4	6	298	0	3.14 ± 0.12	21.39 ± 0.11	21.29	0.9894	1.82	4.26	13.62 ± 0.63	538.87 ± 3.07	555	0.9777	1.65	4.05
15	25	4	6	298	0	1.62 ± 0.06	42.96 ± 0.21	42.37	0.9919	1.32	3.63	22.48 ± 1.91	359.11 ± 2.13	360	0.9802	1.65	4.06
10	25	2	6	298	0	1.24 ± 0.02	27.04 ± 0.07	26.80	0.9956	0.65	2.56	11.80 ± 0.31	676.86 ± 2.08	675	0.9922	0.67	2.60
10	25	3	6	298	0	1.44 ± 0.04	30.68 ± 0.14	29.85	0.9906	1.27	3.56	13.76 ± 0.55	512.22 ± 2.73	520	0.9807	1.55	3.94
10	25	4	8	298	0	1.63 ± 0.05	38.43 ± 0.17	37.30	0.9867	1.82	4.27	15.23 ± 0.65	481.94 ± 2.64	480	0.9701	2.19	4.68
10	25	4	4	298	0	1.44 ± 0.05	19.38 ± 0.23	19.56	0.9814	2.23	4.71	13.36 ± 0.42	243.73 ± 2.45	230	0.9834	1.42	3.73
10	25	4	6	318	0	0.94 ± 0.02	45.98 ± 0.24	45.13	0.9916	1.16	3.40	08.67 ± 0.21	578.44 ± 2.76	580	0.9895	0.80	2.83
10	25	4	6	308	0	1.26 ± 0.02	35.83 ± 0.13	35.34	0.9950	0.67	2.59	11.94 ± 0.24	449.27 ± 1.65	452	0.9784	0.55	2.35
10	25	4	6	298	0.1	2.99 ± 0.04	06.53 ± 0.08	06.88	0.9906	1.23	3.50	29.13 ± 1.10	81.71 ± 1.25	80	0.9906	1.64	4.05
10	25	4	6	298	0.01	1.30 ± 0.04	28.66 ± 0.23	27.50	0.9824	0.86	4.82	11.21 ± 0.35	360.24 ± 2.47	370	0.9834	1.32	3.64

4.2. Bohart–Adams and Wolborska models

The Bohart–Adams and Wolborska models offer a simple and comprehensive approach to evaluate the dynamics of the columns, meanwhile, their validity is limited to the range of conditions used. According to Table 5, the values of the Wolborska model's kinetic constant is found to be influenced by all the studied parameters. This shows that the system is dominated by external mass transfer in the initial part of the sorption process [101]. The parameter β_a reflects the effect of mass transfer in the liquid phase and axial dispersion. The increase in flow rate from 2 to 4 mL min^{-1} increased the value of β_a because the rise in turbulence reduces the film boundary surrounding the absorbent particle [3]. The ratio $\frac{\beta_a}{N_0}$ is equal to K_{BA}, which proves that the expression of Wolborska's solution is equivalent to the Bohart–Adams relationship. Moreover, the correlation coefficient is for the most part effects greater than 0.90 and the error functions not exceeding 2% which also justified the good fit with the adsorption processes and clearly reflect the applicability of the two models.

4.3. BDST model

The bed height and BDST constants are listed in Table 6. Fig. 17 shows that the plots of the service time (t_b) at 10%, 30%, 50%, 70%, and 90% breakthrough points, that is, tb at C_t/C_0 equal to 0.1, 0.3, 0.5, 0.7, and 0.9, respectively. All the R^2 coefficients exceeded 0.99, indicating that the BDST model could be used to represent the adsorption of BF in the PSP fixed-bed column. At $\frac{C_b}{C_0}$ about 0.3, 0.5, 0.7 and 0.9, K_{AB} was abnormal and had negative values, which could be due to the limitation of the BDST model. The obtained results are in agreement with previous studies [54].

5. Regeneration

The desorption of BF molecules adsorbed in the PSP bed column was realized by washing with distilled water. The regenerated PSP bed column was reused to adsorb BF. As can be seen in Figs. 18 and 19 which represent the adsorption/desorption cycles of BF, after column adsorption, the regeneration of PSP fixed bed was carried for two cycles. It was found that the adsorption capacity for BF was reduced after each cycle. The decrease in removal efficiency can be attributed to the loss of partial reduction property of PSP during adsorption–desorption processes [63]. The adsorption efficiency decreased from 68.85% to 27.22% after the third adsorption.

6. Conclusion

PSP was valorized and used as an efficient adsorbent for the removal of BF from water in a dynamic system. The characterization showed that PSP is rich with cellulose, hemicellulose, lignin, and xylene and it exhibits a morphology of hollow cavities with a high roughness that is favorable to the binding organic molecules. Zeta potential of 2.30 mV confirms a positive charge of its surface which is in good agreement with the curve pH_{PZC}. Adsorption measurements

Table 5
Parameters of Bohart–Adams and Wolborska models for BF adsorption by PSP at different conditions using non-linear regression

						Bohart–Adams model						Wolborska model					
C_0 (mg L^{-1})	Z (mm)	F (mL min^{-1})	pH	T (K)	NaCl (N)	$K_{BA} \times 10^3$ (ml mg^{-1} min^{-1})	N_0 (mg L^{-1})	N_{exp} (mg L^{-1})	R^2	$\chi^2 \times 10^3$	ESD (%)	β_a (min^{-1})	N_0 (mg L^{-1})	N_{exp} (mg L^{-1})	R^2	$\chi^2 \times 10^3$	ESD (%)
10	15	4	6	298	0	2.37 ± 0.19	6,328.70 ± 255.89	6,619.56	0.9158	0.26	1.63	15.22 ± 0.66	6,161.43 ± 264.03	6,619.56	0.9100	0.25	1.60
10	25	4	6	298	0	1.44 ± 0.07	8,382.67 ± 143.57	7,752.42	0.9642	0.19	1.38	12.30 ± 0.68	8,269.16 ± 293.42	7,752.42	0.9072	0.20	1.42
10	35	4	6	298	0	0.87 ± 0.05	9,026.86 ± 227.78	7,923.46	0.9397	0.23	1.54	08.05 ± 0.42	8,888.20 ± 330.07	7,923.46	0.9071	0.25	1.58
5	25	4	6	298	0	2.86 ± 0.15	5,488.01 ± 75.30	4,125.96	0.9740	0.12	1.11	15.90 ± 0.84	5,454.80 ± 109.56	4,125.96	0.9601	0.12	1.13
15	25	4	6	298	0	0.70 ± 0.03	14,009.42 ± 314.15	12,316.86	0.9443	0.21	1.44	10.03 ± 0.32	13,772.90 ± 331.95	12,316.86	0.9394	0.20	1.42
10	25	2	6	298	0	0.72 ± 0.04	7,984.51 ± 204.29	7,976.19	0.9540	0.18	1.35	05.93 ± 0.34	7,783.73 ± 305.73	7,976.19	0.9241	0.18	1.36
10	25	3	6	298	0	0.95 ± 0.06	8,030.37 ± 501.67	7,595.41	0.9001	0.47	2.04	07.68 ± 0.59	8,028.52 ± 500.53	7,595.41	0.8663	0.41	2.04
10	25	4	8	298	0	1.06 ± 0.91	9,789.63 ± 379.19	7,643.44	0.9189	0.23	1.54	10.78 ± 0.60	9,368.37 ± 409.22	7,643.44	0.9127	0.22	1.48
10	25	4	4	298	0	1.70 ± 0.16	5,036.65 ± 239.61	6,434.21	0.9264	0.29	1.70	08.64 ± 0.53	4,935.53 ± 344.43	6,434.21	0.8844	0.31	1.76
10	25	4	6	318	0	0.93 ± 0.05	11,239.30 ± 244.02	7,326.29	0.9552	0.20	1.43	11.54 ± 0.37	10,369.86 ± 198.63	7,326.29	0.9584	0.10	1.04
10	25	4	6	308	0	1.22 ± 0.07	9,140.23 ± 208.27	7,362.50	0.9628	0.16	1.29	11.25 ± 0.55	9,027.14 ± 299.49	7,362.50	0.9393	0.18	1.34
10	25	4	6	298	0.1	6.43 ± 0.54	1,201.64 ± 52.21	5,375.00	0.9570	0.23	1.53	08.12 ± 0.44	1,095.89 ± 69.81	5,375.00	0.9371	0.21	1.46
10	25	4	6	298	0.01	0.87 ± 0.06	8,113.73 ± 341.51	6,916.49	0.9215	0.45	2.12	07.07 ± 0.32	8,226.01 ± 565.58	6,916.49	0.8564	0.48	2.19

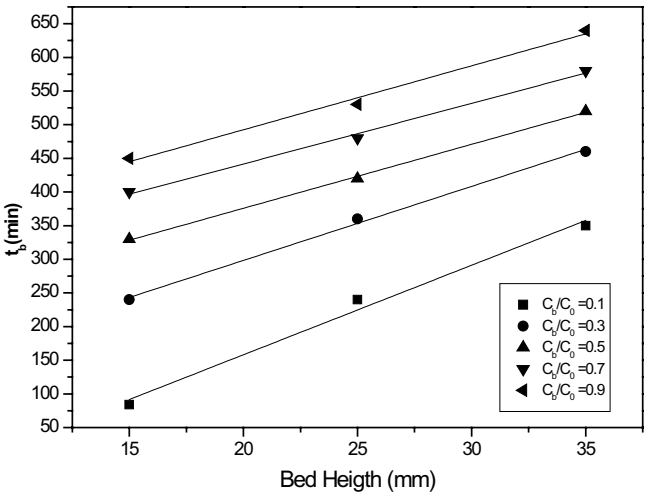

Fig. 17. Linear regression of the BDST model at different breakthrough points. (C_0 = 10 mg L^{-1} and F = 4 mL L^{-1}).

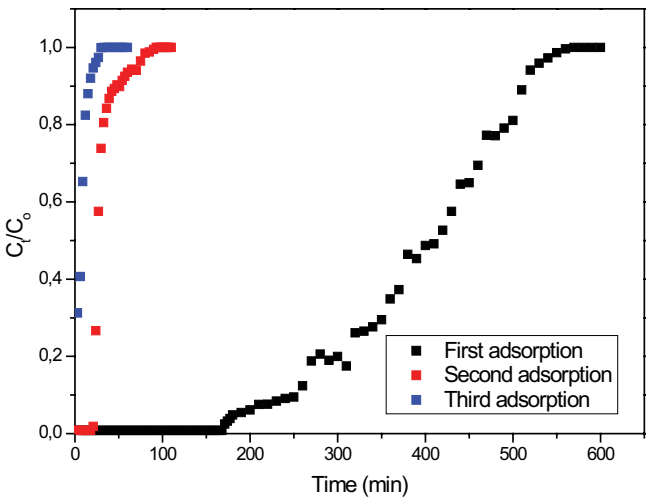

Fig. 18. Breakthrough curves for regenerated PSP. (F = 4 mL min^{-1}, Z = 25 mm, C_0 = 10 mg L^{-1}, and T = 298 ± 1 K).

Table 6
Calculated constants of the BDST model for adsorption of BF. (C_0 = 10 mg L^{-1} and F = 4 mL L^{-1})

$\frac{C_b}{C_0}$	a (min cm^{-1})	b (min)	$K_{AB} \times 10^3$ (L mg^{-1} min^{-1})	N_0' (mg L^{-1})	R^2
0.1	13.30 ± 1.32	–107.833 ± 34.92	2.037	6,777.015	0.9901
0.3	11.00 ± 0.57	78.333 ± 15.18	–4.298	5,605.050	0.9972
0.5	9.50 ± 0.28	185.833 ± 7.59	–2.094	4,840.725	0.9990
0.7	9.00 ± 0.57	261.666 ± 15.18	–1.618	4,585.950	0.9959
0.9	9.50 ± 0.86	302.500 ± 22.77	–1.483	4,840.725	0.9917

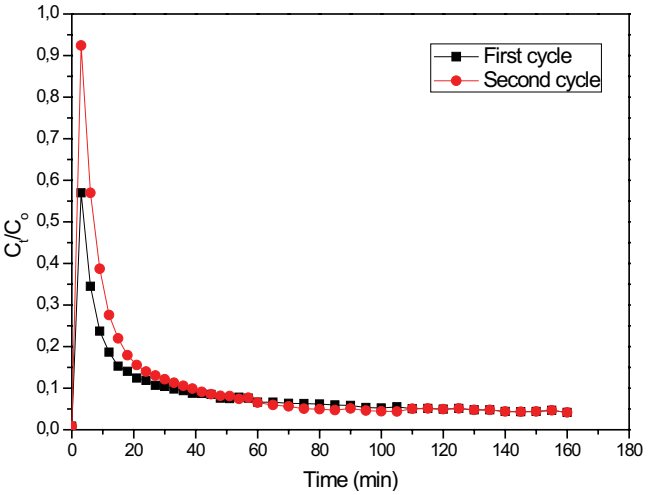

Fig. 19. Desorption of BF from PSP column using distilled water. (F = 4 mL min^{-1}, Z = 25 mm, C_0 = 10 mg L^{-1}, and T = 298 ± 1 K).

carried out by varying experimental conditions indicate that an optimal adsorption efficiency of 98% can be achieved at a flow rate of 4 mL min^{-1}, an initial concentration of 5 mg L^{-1}, a bed height of 55 mm, a pH 6 and a temperature of 298 K. The five adopted models, Thomas, Yoon–Nelson, Bohart–Adams, Wolborska, and BDST were found to be appropriate to describe partially/fully curve of the dynamic behavior of the column. The obtained results highlight the importance of PSP as potential bioadsorbent and can be proposed for the removal of other organics and non-organics contaminants, such as pharmaceuticals products and dyes.

Acknowledgment

The authors acknowledge the financial support of Algerian Ministry of Higher Education.

Symbols

C_0	—	Initial BF concentration, mg L^{-1}
C_t	—	Effluent BF concentration, mg L^{-1}
V_{eff}	—	Effluent volume, mL
F	—	Influent flow rate, mL mn^{-1}
t_e	—	Time of exhaustion, min
t_b	—	Time at breakthrough, min
q_{total}	—	Total weight of BF adsorbed by adsorbent in column, mg
q_{exp}	—	Weight of BF adsorbed per g of adsorbent from experiment, mg g^{-1}
m	—	Adsorbent mass, g

N_{exp} — Experimental maximum sorption capacity, mg L^{-1}
V — Volume of solution, mL
R — Percentage of removal, %
W_{total} — Total amount of BF sent to column, mg
C_{ads} — Adsorbed BF concentration, mg L^{-1}
t — Service time of the column, min
K_{th} — Kinetic constant of Thomas model, L mg^{-1} min^{-1}
q_{th} — Thomas adsorption capacity, mg g^{-1}
U — Linear velocity, mm min^{-1}
K_{YN} — Kinetic constant of Yoon–Nelson model, min^{-1}
K_{BA} — Kinetic constant of Bohart–Adams model, L mg^{-1} min^{-1}
Z — Height of the bed, mm
N_0 — Maximum sorption capacity, mg L^{-1}
C_b — Breakthrough concentration, mg L^{-1}
N_0' — Adsorption capacity in BDST model, mg L^{-1}
T — Temperature, °C, K
pH_{PZC} — pH of point of zero charge
pH_i — Initial pH of the solution
pH_f — Final pH of the solution
ΔpH — Difference between pH_f and pH_i

Greek

τ — Time required for 50% adsorbate breakthrough from Yoon–Nelson model, min
β_a — Kinetic coefficient of the external mass transfer in the Wolborska model, min^{-1}

References

[1] S. Merouani, O. Hamdaoui, Computational and experimental sonochemistry, Process Eng. J., 1 (2017) 10–18.
[2] M. El Haddad, Removal of basic Fuchsin dye from water using mussel shell biomass waste as an adsorbent: equilibrium, kinetics, and thermodynamics, J. Taibah Univ. Sci., 10 (2016) 664–674.
[3] O. Hamdaoui, Dynamic sorption of methylene blue by cedar sawdust and crushed brick in fixed bed columns, J. Hazard. Mater., 138 (2006) 293–303.
[4] V.K. Gupta, A. Mittal, V. Gajbe, J. Mittal, Adsorption of basic fuchsin using waste materials — bottom ash and deoiled soya — as adsorbents, J. Colloid Interface Sci., 319 (2008) 30–39.
[5] L.G. Luna, Manual of Histologic Staining Methods of the Armed Forces Institute of Pathology, McGraw-Hill, New York, 1968.
[6] G.H. Ball, Studies on paramecium, Biol. Bull., 52 (1927) 68–78.
[7] A.A. Fisher, Irritant and toxic reactions to phenol in topical medications, Cutis, 26 (1980) 363–4, 390–2.
[8] V. Burke, C.E. Skinner, The reverse selective bacteriostatic action of acid fuchsin, J. Exp. Med., 37 (1923) 1–10.
[9] N.A. Littlefied, B.N. Blackwell, C.C. Hewit, D.W. Gaylor, Chronic toxicity and carcinogenicity studies of gentian violet in mice, Toxicol. Sci., 5 (1985) 902–912.
[10] S.C.F. Rogers, D. Burrows, D. Neill, Percutaneous absorption of phenol and methyl alcohol in Magenta Paint B.P.C., Br. J. Dermatol., 98 (1978) 559–560.
[11] J. Crookham, J.R. Dapson, Hazardous Chemicals in the Histopathology Laboratory, 2nd ed., Anatech, San Diego, CA, 1991.
[12] F.L. Carson, Histotechnology: A Self-Instructional Text, 2nd ed., American Society Clinical Pathology, Chicago, 1997.
[13] W.J. Weber, Physicochemical Processes for Water Quality Control, Wiley–Interscience, New York, 1972.
[14] M. Kornaros, G. Lyberatos, Biological treatment of wastewaters from a dye manufacturing company using a trickling filter, J. Hazard. Mater., 136 (2006) 95–102.
[15] R.H. Lindberg, U. Olofsson, P. Rendahl, M.I. Johansson, M. Tysklind, B.A.V. Andersson, Behavior of fluoroquinolones and trimethoprim during mechanical, chemical, and active sludge treatment of sewage water and digestion of sludge, Environ. Sci. Technol., 40 (2006) 1042–1048.
[16] T.-H. Kim, C. Park, J. Yang, S. Kim, Comparison of disperse and reactive dye removals by chemical coagulation and Fenton oxidation, J. Hazard. Mater., 112 (2004) 95–103.
[17] C. Chen, Q. Wang, P. Lei, W. Song, W. Ma, J. Zhao, Photodegradation of dye pollutants catalyzed by porous $K_3PW_{12}O_{40}$ under visible irradiation, Environ. Sci. Technol., 40 (2006) 3965–3970.
[18] J. Zhao, C. Chen, W. Ma, Photocatalytic degradation of organic pollutants under visible light irradiation, Top. Catal., 35 (2005) 269–278.
[19] P. Cañizares, F. Martínez, C. Jiménez, J. Lobato, M.A. Rodrigo, Coagulation and electrocoagulation of wastes polluted with dyes, Environ. Sci. Technol., 40 (2006) 6418–6424.
[20] H. Lachheb, E. Puzenat, A. Houas, M. Ksibi, E. Elaloui, C. Guillard, J.-M. Herrmann, Photocatalytic degradation of various types of dyes (Alizarin S, Crocein Orange G, Methyl Red, Congo Red, Methylene Blue) in water by UV-irradiated titania, Appl. Catal., B, 39 (2002) 75–90.
[21] K. Matis, A. Zouboulis, A.I. Zouboulis, A.V. Valtadorou, Sorption of As(V) by goethite particles and study of their flocculation, Water Air Soil Pollut., 111 (1999) 297–316.
[22] A. Ramesh, D.J. Lee, J.W.C. Wong, Thermodynamic parameters for adsorption equilibrium of heavy metals and dyes from wastewater with low-cost adsorbents, J. Colloid Interface Sci., 291 (2005) 588–592.
[23] A. Mittal, V. Thakur, V. Gajbe, Evaluation of adsorption characteristics of an anionic azo dye Brilliant Yellow onto hen feathers in aqueous solutions, Environ. Sci. Pollut. Res., 19 (2012) 2438–2447.
[24] A. Mittal, V. Thakur, V. Gajbe, Adsorptive removal of toxic azo dye Amido Black 10B by hen feather, Environ. Sci. Pollut. Res., 20 (2013) 260–269.
[25] A. Mittal, V. Thakur, J. Mittal, H. Vardhan, Process development for the removal of hazardous anionic azo dye Congo red from wastewater by using hen feather as potential adsorbent, Desal. Water Treat., 52 (2014) 227–237.
[26] A. Mittal, D. Jhare, J. Mittal, Adsorption of hazardous dye Eosin Yellow from aqueous solution onto waste material De-oiled Soya: isotherm, kinetics and bulk removal, J. Mol. Liq., 179 (2013) 133–140.
[27] M. Suzuki, Fundamentals of Adsorption, Proceedings of the Fifth International Conference on Fundamentals of Adsorption, Kyoto, May 17–22, 1992, Kodansha, 1993.
[28] D.M. Ruthven, Principles of Adsorption and Desorption Processes, Wiley, New York, 1984.
[29] M. Zamouche, O. Hamdaoui, Sorption of Rhodamine B by cedar cone: effect of pH and ionic strength, Energy Procedia, 18 (2012) 1228–1239.
[30] E.-K. Guechi, O. Hamdaoui, Cattail leaves as a novel biosorbent for the removal of malachite green from liquid phase: data analysis by non-linear technique, Desal. Water Treat., 51 (2013) 3371–3380.
[31] N. Nasuha, B.H. Hameed, A.T.M. Din, Rejected tea as a potential low-cost adsorbent for the removal of methylene blue, J. Hazard. Mater., 175 (2010) 126–132.
[32] O. Hamdaoui, Intensification of the sorption of Rhodamine B from aqueous phase by loquat seeds using ultrasound, Desalination, 271 (2011) 279–286.
[33] S. Boutemedjet, O. Hamdaoui, Sorption of malachite green by eucalyptus bark as a non-conventional low-cost biosorbent, Desal. Water Treat., 8 (2009) 201–210.
[34] M. Zamouche, O. Hamdaoui, A use of cedar cone for the removal of a cationic dye from aqueous solutions by sorption, Energy Procedia, 18 (2012) 1047–1058.

[35] D. Sud, G. Mahajan, M.P. Kaur, Agricultural waste material as potential adsorbent for sequestering heavy metal ions from aqueous solutions – a review, Bioresour. Technol., 99 (2008) 6017–6027.
[36] C. Djelloul, O. Hamdaoui, Removal of cationic dye from aqueous solution using melon peel as nonconventional low-cost sorbent, Desal. Water Treat., 52 (2014) 7701–7710.
[37] B.D. Bhole, B. Ganguly, A. Madhuram, D. Deshpande, J. Joshi, Biosorption of methyl violet, basic fuchsin and their mixture using dead fungal biomass, Curr. Sci., 86 (2004) 1641–1645.
[38] S.Y. An, S.K. Min, I.H. Cha, Y.L. Choi, Y.S. Cho, C.H. Kim, Y.C. Lee, Decolorization of triphenylmethane and azo dyes by *Citrobacter* sp., Biotechnol. Lett., 24 (2002) 1037–1040.
[39] E.O. Oyelude, F. Frimpong, D. Dawson, Studies on the removal of basic fuchsin dye from aqueous solution by HCl treated malted sorghum mash, J. Mater. Environ. Sci., 6 (2015) 1126–1136.
[40] P. Duo-Hai, Z. Peng-Xiang, L. Xiang-Sheng, M. Run-Cai, H. Yi-Xian, A study on surface-enhanced hyper-raman scattering of basic fuchsin adsorbed on the silver colloid, Acta Phys. Sin., Overseas Ed., 2 (1993) 925–929.
[41] L. Huang, J. Kong, W. Wang, C. Zhang, S. Niu, B. Gao, Study on Fe(III) and Mn(II) modified activated carbons derived from *Zizania latifolia* to removal basic fuchsin, Desalination, 286 (2012) 268–276.
[42] S. Kalita, M. Pathak, G. Devi, H.P. Sarma, K.G. Bhattacharyya, A. Sarma, A. Devi, Utilization of *Euryale ferox* Salisbury seed shell for removal of basic fuchsin dye from water: equilibrium and kinetics investigation, RSC Adv., 7 (2017) 27248–27259.
[43] B. Kizilkaya, Usage of biogenic apatite (Fish Bones) on removal of Basic Fuchsin dye from aqueous solution, J. Dispersion Sci. Technol., 33 (2012) 1596–1602.
[44] J. Kong, L. Huang, Q. Yue, B. Gao, Preparation of activated carbon derived from leather waste by H_3PO_4 activation and its application for basic fuchsin adsorption, Desal. Water Treat., 52 (2014) 2440–2449.
[45] X. Zhuang, Y. Wan, C. Feng, Y. Shen, D. Zhao, Highly efficient adsorption of bulky dye molecules in wastewater on ordered mesoporous carbons, Chem. Mater., 21 (2009) 706–716.
[46] Y. Zhou, Q. Jin, X. Hu, Heavy metal ions and organic dyes removal from water by cellulose modified with maleic anhydride, J. Sci. Mater., 47 (2012) 5019–5029.
[47] H. Tavallali, A. Daneshyar, Modified iron oxide nanoparticles as solid phase extractor for spectrophotometeric determination and separation of muroxide, Int. J. ChemTech Res., 4 (2012) 1170–1173.
[48] R. Li, Y. Zhang, W. Chu, Z. Chen, J. Wang, Adsorptive removal of antibiotics from water using peanut shells from agricultural waste, RSC Adv., 8 (2018) 13546–13555.
[49] V. Ponnusami, V. Gunasekar, S.N. Srivastava, Kinetics of methylene blue removal from aqueous solution using gulmohar (*Delonix regia*) plant leaf powder: Multivariate regression analysis, J. Hazard. Mater., 169 (2009) 119–127.
[50] E. Malkoc, Y. Nuhoglu, Removal of Ni(II) ions from aqueous solutions using waste of tea factory: adsorption on a fixed-bed column, J. Hazard. Mater., 135 (2006) 328–336.
[51] J. López-Cervantes, D.I. Sánchez-Machado, R.G. Sánchez-Duarte, M.A. Correa-Murrieta, Study of a fixed-bed column in the adsorption of an azo dye from an aqueous medium using a chitosan–glutaraldehyde biosorbent, Adsorpt. Sci. Technol., 36 (2018) 215–232.
[52] A.A. Ahmad, B.H. Hameed, Fixed-bed adsorption of reactive azo dye onto granular activated carbon prepared from waste, J. Hazard. Mater., 175 (2010) 298–303.
[53] W. Zhang, L. Dong, H. Yan, H. Li, Z. Jiang, X. Kan, H. Yang, A. Li, R. Cheng, Removal of methylene blue from aqueous solutions by straw based adsorbent in a fixed-bed column, Chem. Eng. J., 173 (2011) 429–436.
[54] E. Oguz, M. Ersoy, Biosorption of cobalt(II) with sunflower biomass from aqueous solutions in a fixed bed column and neural networks modelling, Ecotoxicol. Environ. Saf., 99 (2014) 54–60.
[55] H.C. Thomas, Heterogeneous ion exchange in a flowing system, J. Am. Chem. Soc., 66 (1944) 1664–1666.
[56] Y.H. Yoon, J.H. Nelson, Application of gas adsorption kinetics. A theoretical model for respirator cartridge service life, Am. Ind. Hyg. Assoc. J., 45 (1984) 509–516.
[57] G.S. Bohart, E.Q. Adams, Some aspects of the behavior of charcoal with respect to chlorine, J. Am. Chem. Soc., 42 (1920) 523–544.
[58] A. Wolborska, Adsorption on activated carbon of *p*-nitrophenol from aqueous solution, Water Res., 23 (1989) 85–91.
[59] R.E. Hassan, E.H. Borai, Fixed bed column study for separation of light lanthanides by dowex-50X8, Int. J. Sci. Eng. Environ., 2 (2011) 101–116.
[60] M. Auta, B.H. Hameed, Coalesced chitosan activated carbon composite for batch and fixed-bed adsorption of cationic and anionic dyes, Colloids Surf., B, 105 (2013) 199–206.
[61] K.Y. Foo, B.H. Hameed, Insights into the modeling of adsorption isotherm systems, Chem. Eng. J., 156 (2010) 2–10.
[62] R. Zerdoum, Z. Hattab, Y. Berredjem, R. Mazouz, R. Djellabi, N. Filali, A. Gheid, K. Guerfi, Removal of methylene blue from water using eggshell membrane fixed bed, Desal. Water Treat., 81 (2017) 252–264.
[63] A. Ahmad, Z.A. Ghazi, M. Saeed, M. Ilyas, R. Ahmad, A.M. Khattak, A. Iqbal, A comparative study of the removal of Cr(VI) from synthetic solution using natural biosorbents, New J. Chem., 41 (2017) 10799–10807.
[64] M.E. Ossman, M.S. Mansour, M.A. Fattah, N. Taha, Y. Kiros, Peanut shells and talc powder for removal of hexavalent chromium from aqueous solutions, Bulg. Chem. Commun., 46 (2014) 629–639.
[65] J. Bossa, F. Borget, F. Duvernay, P. Theule, T. Chiavassa, Formation of neutral methylcarbamic acid ($CH_3NHCOOH$) and methylammonium methylcarbamate [CH_3NH^{3+}][CH_3NHCO^{2-}] at low temperature, J. Phys. Chem. A, 112 (2008) 5113–5120.
[66] A. Danon, P.C. Stair, E. Weitz, FTIR study of CO_2 adsorption on amine-grafted SBA-15: elucidation of adsorbed species, J. Phys., 115 (2011) 11540–11549.
[67] C. Knöfel, C. Martin, V. Hornebecq, P.L. Llewellyn, Study of carbon dioxide adsorption on mesoporous aminopropylsilane-functionalized silica and titania combining microcalorimetry and in situ infrared spectroscopy, J. Phys., 113 (2009) 21726–21734.
[68] N. Quaranta, Use of wastes from the peanut industry in the manufacture of building materials, Int. J. Sustainable Dev. Plann., 13 (2018) 662–670.
[69] S. Boumchita, Y. Benjelloun, V. Nenov, F. Zerrouq, Application of Peanut shell as a low-cost adsorbent for the removal of anionic dye from aqueous solutions, J. Mater. Environ. Sci., 8 (2017) 2353–2364.
[70] C.S. Zhu, L.P. Wang, W.B. Chen, Removal of Cu(II) from aqueous solution by agricultural by-product: peanut hull, J. Hazard. Mater., 168 (2009) 739–746.
[71] R. Gong, Y. Sun, J. Chen, H. Liu, C. Yang, Effect of chemical modification on dye adsorption capacity of peanut hull, Dyes Pigm., 67 (2005) 175–181.
[72] L.C.V. Ítavo, C.M. Soares, C.C.B.F. Ítavo, A.M. Dias, H.V. Petit, E.S. Leal, A.D.V. De Souza, Calorimetry, chemical composition and in vitro digestibility of oilseeds, Food Chem., 185 (2015) 219–225.
[73] A. Sonia, K.P. Dasan, Chemical, morphology and thermal evaluation of cellulose microfibers obtained from *Hibiscus sabdariffa*, Carbohydr. Polym., 92 (2013) 668–674.
[74] G.F. Malash, M.I. El-Khaiary, Methylene blue adsorption by the waste of Abu-Tartour phosphate rock, J. Colloid Interface Sci., 348 (2010) 537–545.
[75] R.M. Ali, H.A. Hamad, M.M. Hussein, G.F. Malash, Potential of using green adsorbent of heavy metal removal from aqueous solutions: adsorption kinetics, isotherm, thermodynamic, mechanism and economic analysis, Ecol. Eng., 91 (2016) 317–332.
[76] H. Yang, R. Yan, H. Chen, D.H. Lee, C. Zheng, Characteristics of hemicellulose, cellulose and lignin pyrolysis, Fuel, 86 (2007) 1781–1788.

[77] R. Djomi, L.J.R. Meva'a, J. Nganhou, G. Mbobda, A.E. Njom, Y.D.M. Bampel, J.B.S. Tchinda, Physicochemical and thermal characterization of dura palm kernel powder as a load for polymers: case of polyvinyl chloride, J. Mater. Sci. Chem. Eng., 6 (2018) 1–18.
[78] X. Xu, B.Y. Gao, X. Tang, Q.Y. Yue, Q.Q. Zhong, Q. Li, Characteristics of cellulosic amine-crosslinked copolymer and its sorption properties for Cr(VI) from aqueous solutions, J. Hazard. Mater., 189 (2011) 420–426.
[79] B.D. Zdravkov, J.J. Čermák, M. Šefara, J. Janků, Pore classification in the characterization of porous materials: a perspective, Cent. Eur. J. Chem., 5 (2007) 385–395.
[80] L.-X. Li, D. Xu, X.-Q. Li, W.-C. Liu, Y.J. De, Excellent fluoride removal properties of porous hollow MgO microspheres, R. Soc. J. Chem., 38 (2014) 5445–5452.
[81] A. Allaoui, Z. Hattab, R. Zerdoum, R. Djellabi, Y. Berredjem, W. Bessashia, K. Guerfi, Adsorption of hexavalent chromium by crushed brick: effect of operating parameters and modeling study, Desal. Water Treat., 131 (2018) 291–304.
[82] R. Mazouz, N. Filali, Z. Hattab, K. Guerfi, Valorization of granulated slag of Arcelor-Mittal (Algeria) in cationic dye adsorption from aqueous solution: column studies, J. Water Reuse Desal., 6 (2016) 204–213.
[83] A.P. Lim, A.Z. Aris, Continuous fixed-bed column study and adsorption modeling: removal of cadmium(II) and lead(II) ions in aqueous solution by dead calcareous skeletons, Biochem. Eng. J., 87 (2014) 50–61.
[84] M.G.A. Vieira, R.M. Oisiovici, M.L. Gimenes, M.G.C. Silva, Biosorption of chromium(VI) using a *Sargassum* sp. packed-bed column, Bioresour. Technol., 99 (2008) 3094–3099.
[85] S. Chen, Q. Yue, B. Gao, Q. Li, X. Xu, K. Fu, Adsorption of hexavalent chromium from aqueous solution by modified corn stalk: a fixed-bed column study, Bioresour. Technol., 113 (2012) 114–120.
[86] J.T. Igbokwe, Adsorption performance of packed bed column for the removal of lead(II) using oil palm fibre, Int. J. Appl. Sci. Technol., 2 (2012) 106–115.
[87] E. Malkoc, Y. Nuhoglu, Fixed bed studies for the sorption of chromium(VI) onto tea factory waste, Chem. Eng. Sci., 61 (2006) 4363–4372.
[88] G. McKay, M. El Geundi, M.M. Nassar, Equilibrium studies during the removal of dyestuffs from aqueous solutions using bagasse pith, Water Res., 21 (1987) 1513–1520.
[89] T. Vickerstaff, The Physical Chemistry of Dyeing, Imperial Chemical Industries, Ltd., London, 1954.
[90] G.S. Gupta, G. Prasad, V.N. Singh Removal of chrome dye from carpet effluents using coal-I, Environ. Technol. Lett., 9 (1988) 153–161.
[91] G.S. Gupta, G. Prasad, V.N. Singh, Removal of chrome dye from aqueous solutions by mixed adsorbents: fly ash and coal, Water Res., 24 (1990) 45–50.
[92] S.K. Khare, R.M. Srivastava, K.K. Panday, V.N. Singh, Removal of basic dye (crystal violet) from water using wollastonite as adsorbent, Environ. Technol. Lett., 9 (1988) 1163–1172.
[93] M.A. Akl, A.F.M. Youssef, A.H. Hassan, H. Maher, Synthesis, characterization and evaluation of peanut shells-derived activated carbons for removal of methomyl from aqueous solutions, Environ. Anal. Toxicol., 6 (2016), doi: 10.4172/2161-0525.1000352.
[94] M. Auta, B.H. Hameed, Chitosan-clay composite as highly effective and low-cost adsorbent for batch and fixed-bed adsorption of methylene blue, Chem. Eng. J., 237 (2014) 352–361.
[95] N. Barka, A. Assabbane, A. Nounah, L. Laanab, Y.A. Ichou, Removal of textile dyes from aqueous solutions by natural phosphate as a new adsorbent, Desalination, 235 (2009) 264–275.
[96] Y.S. Al-degs, M.I. El-barghouthi, A.H. El-sheikh, G.M. Walker, Effect of solution pH, ionic strength, and temperature on adsorption behavior of reactive dyes on activated carbon, J. Dyes Pigm., 77 (2008) 16–23.
[97] D. Ozer, A. Ozer, Methylene blue adsorption from aqueous solution by dehydrated peanut hull, J. Hazard. Mater., 144 (2007) 171–179.
[98] Y. Song, S. Chen, Y. Gao, H. Xu, Fuchsine adsorption from aqueous solution by epichlorohydrin crosslinked peanut husk, Adv. Mater. Res., 549 (2012) 362–365.
[99] Z. Aksu, F. Gönen, Biosorption of phenol by immobilized activated sludge in a continuous packed bed: prediction of breakthrough curves, Process Biochem., 39 (2004) 599–613.
[100] A. Singh, D. Kumar, J.P. Gaur, Continuous metal removal from solution and industrial effluents using *Spirogyra* biomass-packed column reactor, Water Res., 46 (2011) 779–788.
[101] Z.Z. Chowdhury, S.M. Zain, A.K. Rashid, R.F. Rafique, K. Khalid, Breakthrough curve analysis for column dynamics sorption of Mn(II) ions from wastewater by using *Mangostana garcinia* peel-based granular-activated carbon, J. Chem., 2013 (2013), doi: 10.1155/2013/959761.